Critical field of Al-doped MgB2 samples: Correlation with the suppression of the sigma-band gap

Critical field of Al-doped MgB_2 samples: Correlation with the suppression of the σ-band gap

M. Putti,[1] C. Ferdeghini,[1] M. Monni,[1] I. Pallecchi,[1] C. Tarantini,[1] P. Manfrinetti,[2] A. Palenzona,[2] D. Daghero,[3] R. S. Gonnelli,[3] and V. A. Stepanov[4]

[1]*INFM-LAMIA, Dipartimento di Fisica, Università di Genova, via Dodecaneso 33, 16146 Genoa, Italy*

[2]*INFM-LAMIA, Dipartimento di Chimica e Chimica Industriale, Università di Genova, via Dodecaneso 33, 16146 Genoa, Italy*

[3]*INFM-LAMIA, Dipartimento di Fisica, Politecnico di Torino, corso Duca degli Abruzzi 24, 10129 Torino, Italy*

[4]*P.N. Lebedev Physical Institute, Russian Academy of Sciences, Leninski Prospekt 53, 119991, Moscow, Russia*

(Received 15 June 2004; revised manuscript received 3 February 2005; published 14 April 2005)

In this paper, a study of the effect of Al substitution on the upper critical field, B_{c2}, in $Al_xMg_{1-x}B_2$ samples is presented. We find a straightforward correlation between B_{c2} and the σ-band gap, Δ_σ, evaluated by point-contact measurements. Up to $x=0.2$, B_{c2} can be well described within a clean limit model and its decrease with x is directly related to the suppression of Δ_σ.

DOI: 10.1103/PhysRevB.71.144505 PACS number(s): 74.70.Ad, 72.15.Lh, 74.25.Jb, 74.25.Op

INTRODUCTION

Superconductivity at 40 K in magnesium diboride has been extensively studied since its discovery.[1] The presence of two bands crossing the Fermi level and having strongly different character[2,3] is well established: two π bands are formed by p_z orbitals of boron and are three-dimensional, electron-type, and weakly coupled with phonons; two σ bands are formed by sp^2-hybrid orbitals stretched along the B-B bonds and are two-dimensional, hole-type, and strongly coupled with the optical E_{2g} phonon mode. This peculiar band structure, joined to the fact that interband scattering by impurities is inhibited by the different parity of π and σ orbitals,[4] is at the ground of the two-gap superconductivity. The lack of interband scattering yields important consequences in the transport behavior because it prevents the mixing of the σ and π carriers, which maintain their own characteristics. This gives a unique chance to selectively disorder each channel independently and offers many opportunities to tune superconducting and normal properties.

Many attempts of selective doping have been carried out. For example, substitution of C in the B site significantly increases the upper critical fields, as reported by several groups,[5–7] suggesting that, in this case, the dirty regime is well stabilized. On the other hand, Al substitution of Mg does not give unequivocal results. In Al-doped single crystals, the critical field perpendicular to the *ab* planes, $B_{c2\perp ab}$, increases with increasing Al concentration, while the one parallel to the *ab* planes, $B_{c2\parallel ab}$, decreases, as observed also in polycrystalline samples.[8] The behavior of $B_{c2\perp ab}$ has been explained within a dirty limit model, but this interpretation clashes with the decreasing of $B_{c2\parallel ab}$. Actually, there are several effects caused by the Al substitution of Mg: the rising of the Fermi level,[9,10] the stiffening of the E_{2g} mode,[11] and the increasing of the interband scattering.[12] The importance of the last effect on the superconducting properties of Al-doped samples has not been clarified yet. Its main signature should be the decrease of the σ-band gap, Δ_σ, together with the increase of the π-band gap, Δ_π; for large interband scattering the gaps should merge to the BCS value.[13] The only available data of gaps as a function of Al (Ref. 14), show a strong decrease of Δ_σ, which could be related to the increased interband scattering, while Δ_π remains rather constant in contrast with expectations.[13]

Both the energy gaps and the scattering rates vary with the doping determining the regime of conduction (clean or dirty) of each band. Thus B_{c2} must depend on Al doping in a nontrivial way and the study of its behavior gives a unique opportunity to investigate the peculiar role of disorder in a two-gap superconductor.

This paper tackles the multifaceted subject of transport regimes in Al-doped samples. We correlated the upper critical fields, the energy gaps, and the scattering rates in a set of polycrystalline $Al_xMg_{1-x}B_2$ samples to investigate the effect of Al substitution on the conduction regimes of σ and π bands.

EXPERIMENT

Dense, clean, and hard cylinder-shaped samples were obtained by direct synthesis of pure elements.[15] In order to improve the homogeneity of doping, Mg-Al alloys were prepared in a first step with Al concentration ranging from 0 to 0.2. In the second step, a cylindrical piece of Mg-Al alloy was put, on crystalline B powders, in Ta crucibles welded in argon and closed in quartz tubes. The quartz tube is then placed in a vertical furnace which is at 850–900 °C. The Mg-Al alloy melts and reacts in the liquid state with the B powders; after 1 h the temperature is raised and maintained at 1000 °C for 100 h. This procedure gives hard cylindrical-shaped bulk samples (12 mm diameter and 10 mm height). XRD analyses made on the top and on the bottom of the cylinder have emphasized that the doped samples present a gradient of Al concentration along the height, being that the top of the sample is less Al doped than the bottom. In the most alloyed samples, the Al concentration was found to vary by about $\Delta x=0.05$ along the height of the sample. Thus each piece of sample, cut at different height, could present a concentration slightly different from the nominal one: for a careful determination of the actual concentration, XRD, as well as critical temperature evaluation, are required. Seven $Al_xMg_{1-x}B_2$ samples were prepared: the samples with $x=0$, 0.10, and 0.15 are prepared with natural B, while the samples with $x=0.05$, 0.07, and 0.20 are prepared with isotopically enriched ^{11}B. Undoped samples made with ^{11}B instead of natural B present lower resistivity, probably due to the higher

TABLE I. Parameters of $Al_xMg_{1-x}B_2$ polycrystalline samples: Al concentration values are $x\pm\Delta x$, where Δx is estimated by the amplitude of resistive transition; the critical temperature is defined as $T_c=(T_{90\%}+T_{10\%})/2$ and $\Delta T_c=(T_{90\%}-T_{10\%})$, where $T_{90\%}$ and $T_{10\%}$ are estimated at 90% and 10% of the resistive transition; ρ_0 is defined as the resistivity measured at 40 K; the residual resistivity ratio is defined as RRR=$\rho(300)/\rho(40)$; the crystallographic a and c axes; the σ-band scattering rate is $\Gamma_\sigma=\Gamma_{\sigma\sigma}+\Gamma_{\sigma\pi}$ given by the sum of intraband ($\Gamma_{\sigma\sigma}$) and interband ($\Gamma_{\sigma\pi}$) scattering rates.

$x\pm\Delta x$	$T_c\pm\Delta T_c/2$(K)	$\rho_0(\mu\Omega$ cm)	RRR	a axis(Å)	c axis(Å)	Γ_σ(meV)	$\frac{\Gamma_\sigma}{\pi\Delta_\sigma}$
0	39.0±0.1	2.5±0.5	7.2	3.085	3.525		
0.05±0.01	36.6±0.5	5.0±0.5	4.7	3.083	3.508	7	0.4
0.07±0.01	35.8±0.5	6.7±0.8	2.7	3.079	3.489	9	0.5
0.10±0.02	33.4±1.5	8±1	2.2	3.077	3.483	10	0.6
0.15±0.02	31.5±1.5	12±1	1.9	3.076	3.456	13	0.9
0.20±0.02	29.1±0.9	7±1	2.1	3.077	3.453	7	0.6

purity of such a boron, but exactly the same upper critical field.[8] Microstructure and chemical composition have been investigated by scanning electron microscopy, electron probe microanalysis, and preliminary transmission electron microscopy.[16] No significant phase separations were detected up to the highest Al concentration: the detected B-rich minority phases were less than 3% in volume in the worst case. Al is incorporated into MgB_2 grains of size ~ 1 μm by substitution of a Mg lattice and becomes rather inhomogeneously distributed with increasing Al concentration. X-ray powder patterns were obtained by a Guinier-Stoe camera. No extra peaks due to the presence of free Mg or spurious phases were detected. Peaks of the doped compounds are shifted in comparison with pure MgB_2 peaks and they broaden on increasing the Al content; the lattice parameters, reported in Table I, are in good agreement with other reports.[14,17]

All the samples were cut in the shape of a parallelepiped bar ($\sim 1\times 2\times 12$ mm^3). Magnetoresistivity measurements were performed from 0 to 9 T in a PPMS Quantum Design system and the undoped sample was measured up to 20.3 T at the Grenoble High Magnetic Field Laboratory, France.

Point-contact measurements (PCM) were carried out by using the "soft" technique described elsewhere,[18] which consists of creating a small (nearly 50 μm diameter) metallic contact on the sample surface by using a drop of Ag paint. With respect to the more usual point-contact technique, which involves a metallic tip pressed against the sample surface, this ensures much greater stability of the contacts on thermal cycling and reproducibility of the results. Moreover, it is more suited for polycrystalline samples with possible local variations in the chemical composition, since, due to the finite size of the contact, it actually provides an average over a certain region in direct space. The average over a portion of the Fermi surface, instead, is intrinsic to the point-contact technique and arises from the finite aperture of the current injection cone. In the case of polycrystalline $Mg_{1-x}Al_xB_2$ samples, with random grain orientation, this allows observing two-gap structures rather easily—which may be very difficult with strictly directional measurements like STM. The low-temperature conductance curves (dI/dV versus V) of the $Ag/Mg_{1-x}Al_xB_2$ point contacts were obtained by numerical differentiation of the measured I-V characteristics, and presented clear structures due to Andreev reflection at the interface, in the form of conductance maxima whose positions give a rough indication of the gap amplitudes.

RESULTS AND DISCUSSION

Figure 1 shows the resistivity as a function of temperature of the $Mg_{1-x}Al_xB_2$ samples with $x=0$, 0.05, 0.07, 0.10, 0.15, and 0.20. The critical temperature T_c, the residual resistivity ρ_0, and the residual resistivity ratio (RRR) are summarized in Table I. We assume an error in the evaluation of resistivity of ±10% due to the uncertainty of the geometrical factor. Moreover, in polycrystals it is critically sensitive to sample density and effective percolation path between grains, which causes an overestimation of resistivity. On the other hand, scanning electron microscope images of our samples show a network of well connected grains,[19] so we assume a negligible contribution of grain boundaries.

The transition width gets larger for more heavily doped samples, where inhomogeneities are more likely to occur, but no multiple transitions were observed (see the inset of Fig. 1). The resistivity values are comparable with the ones reported for Al-doped single crystals,[20] indicating the excellent quality of this set of samples. ρ_0 increases monotonically with the doping, ranging from 2.5 $\mu\Omega$ cm to 12 $\mu\Omega$ cm, apart from the $x=0.20$ sample, made with ^{11}B, which has a ρ_0 value lower than the $x=0.10$ and $x=0.15$ samples.

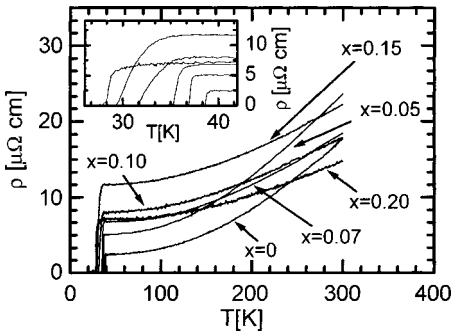

FIG. 1. Resistivity as a function of temperature for the $Al_xMg_{1-x}B_2$ samples ($x=0$, 0.05, 0.07, 0.10, 0.15, 0.20). In the inset, the temperature region close to the transition is magnified.

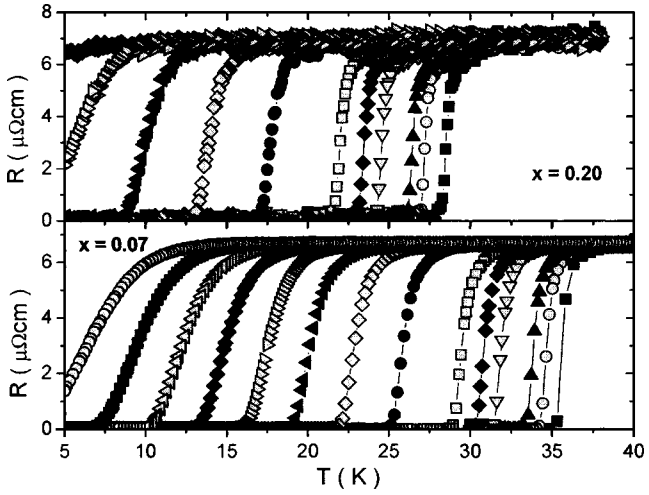

FIG. 2. Magnetoresistivity curves as a function of temperature at a fixed magnetic field. Lower panel: $x=0.07$ sample, B=0, 0.1, 0.2, 0.5, 0.7, 1, 2, 3, 4, 5, 6, 7, 8, and 9 T. Higher panel: $x=0.20$ sample, same fields up to 6 T.

Figure 2 shows, as an example, the magnetoresistivity curves of the $x=0.07$ and 0.20 samples measured at a fixed field and varying the temperature. The upper critical field curve $B_{c2}(T)$ was operatively defined as 90% of these curves. Our criterion provides the determination of the uppermost $B_{c2}(T)$ curve, which is $B_{c2\|ab}$ for the pure polycrystalline samples (Ref. 6 and references therein); in substituted compounds which present some inhomogeneities, our criterion probes the grains with a lower level of doping.

Increasing disorder in single-gap superconductors is usually accompanied by an increase in the upper critical field.[21] In the left panel of Fig. 3, B_{c2} is plotted as a function of temperature for all the samples considered here. As is clearly seen, B_{c2} monotonically decreases with increasing Al concentration; this monotonic trend is maintained even if B_{c2} is plotted as a function of the reduced temperature T/T_c, as seen in the right panel of Fig. 3. Measurements on Al-doped single crystals show indeed that the critical field decreases

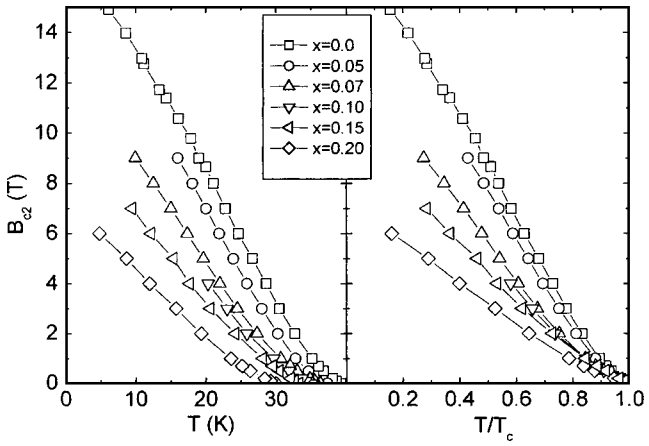

FIG. 3. Left panel: B_{c2} of the $Al_xMg_{1-x}B_2$ samples as a function of temperature; right panel: B_{c2} of the $Al_xMg_{1-x}B_2$ samples as a function of the reduced temperature T/T_c.

with doping when the external field is parallel to the *ab* planes.[20] In Ref. 8, we showed that at a low level of doping ($x<0.1$), this unusual behavior is explained assuming that, in spite of the disorder introduced by Al doping, the B_{c2} can be described within a clean-limit model.

In the clean limit, the critical fields of MgB_2 at low temperature are determined by the σ bands.[22,23] Thus, far from the transition, the critical fields perpendicular and parallel to the *ab* planes can be expressed in terms of the coherence lengths of the σ carriers in either direction, $\xi_{0_{\sigma ab}}$ or $\xi_{0_{\sigma c}}$,

$$B_{c2\perp ab}(T)=\frac{\Phi_0}{2\pi\xi_{0_{\sigma ab}}(T)^2}, \tag{1a}$$

$$B_{c2\|ab}(T)=\frac{\Phi_0}{2\pi\xi_{0_{\sigma ab}}(T)\xi_{0_{\sigma c}}(T)}. \tag{1b}$$

By inserting $\xi_{0_{\sigma j}}=\hbar v_{F_{\sigma j}}/\pi\Delta_\sigma$ and $\Phi_0=2.07\times10^{-15}$ T m^2, we can express the upper critical fields and the anisotropy γ as a function of Δ_σ and of the in-plane, $\nu_{F_{\sigma ab}}$, and out-of-plane, $\nu_{F_{\sigma c}}$, Fermi velocities of σ bands,

$$B_{c2\perp ab}(T)=\frac{\Phi_0\pi\Delta_\sigma(T)^2}{2\hbar^2(\nu_{F_{\sigma ab}})^2}, \tag{2a}$$

$$B_{c2\|ab}(T)=\frac{\Phi_0\pi\Delta_\sigma(T)^2}{2\hbar^2\nu_{F_{\sigma ab}}v_{F_{\sigma c}}}, \tag{2b}$$

$$\gamma=B_{c2\|ab}/B_{c2\perp ab}=\nu_{F_{\sigma ab}}/\nu_{F_{\sigma c}}. \tag{2c}$$

Therefore, to analyze the upper critical fields, it is necessary to consider the changes in the electronic structure and in the energy gaps due to Al doping.

Doping with Al makes the topology of the σ Fermi surface change: at $x=0.33$, the complete filling of the σ bands at the Γ point occurs, and a crossover happens from a two-dimensional to a three-dimensional dispersion regime.[9,10,24]

The Fermi velocities of the σ bands, defined by

$$\nu_{F_{\sigma i}}^2=\left\langle\left(\frac{\partial\varepsilon(\vec{k})}{\partial k_i}\right)^2\right\rangle_{FS,\sigma}\quad(i=ab,c),$$

have been calculated by averaging squared velocities over the Fermi surface sheets of the σ bands. We used the electronic structure $\varepsilon(\vec{k})$ at various Al contents calculated *ab initio* by Profeta *et al.*[10] The Fermi velocities vary with Al doping as shown in the upper panel of Fig. 4: $\nu_{F_{\sigma ab}}$ decreases with increasing x while $\nu_{F_{\sigma c}}$ increases. Thus the critical fields are affected in different ways by the changes in the Fermi velocities: $B_{c2\|ab}$ is only slightly affected, while $B_{c2\perp ab}$ has to increase and the anisotropy γ decrease ($\gamma\approx6$ at $x=0$ and $\gamma\approx3$ at $x=0.4$). Noticeably, an increase of $B_{c2\perp ab}$ as well as a decrease of γ with Al doping have been recently reported in single crystals.[20]

Equations (2a) and (2b) show a quadratic dependence on Δ_σ, thus the σ-gap determination as a function of doping becomes essential. Here the gap energies have been evalu-

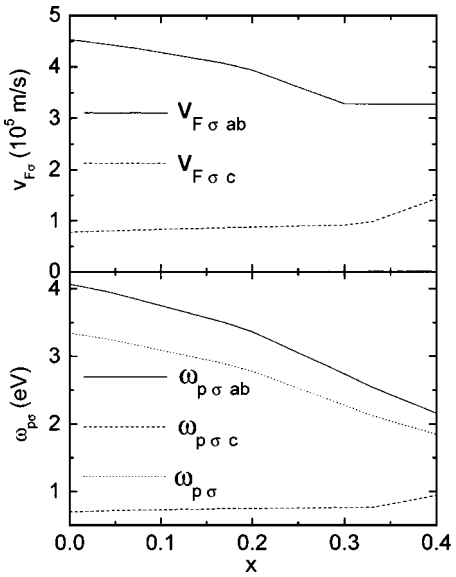

FIG. 4. $\nu_{F_{\sigma ab}}$ and $\nu_{F_{\sigma c}}$ as a function of x (upper panel); $\omega_{p_{\sigma ab}}$, $\omega_{p_{\sigma c}}$ and the spatial average ω_{p_σ} as a function of x (lower panel).

ated by PCM, with the technique described above. Representative low-temperature conductance curves measured in $Mg_{1-x}Al_xB_2$ samples with $x=0$, 0.1, and 0.2 are reported in Fig. 5. The fulfillment of the conditions for ballistic conduction across the junction (at least at 4.2 K) is witnessed by the

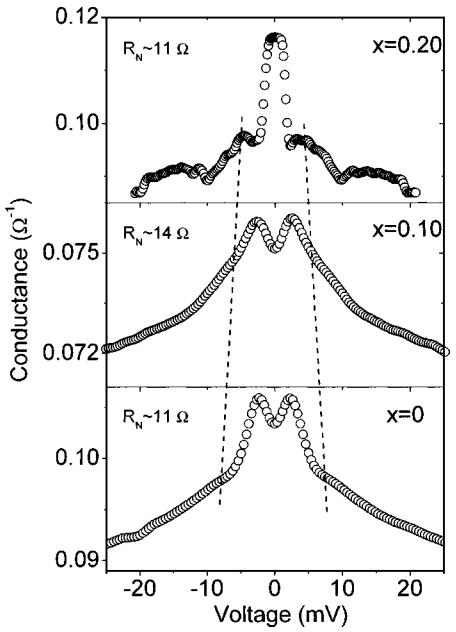

FIG. 5. Examples of low-temperature (4.2 K) non-normalized (i.e., as-measured) conductance curves of Ag-spot point contacts on $Mg_{1-x}Al_xB_2$ samples with (from bottom to top) $x=0$, $x=0.1$, and $x=0.2$. The straight dashed line indicates that the structure related to the large gap Δ_σ (a shoulder in the first two cases, and a small peak in the third) moves toward lower energies on increasing the Al content. This is suggestive of the corresponding reduction in the value of the gap amplitude obtained from the fit of the normalized curves.

rather flat background and the absence of the typical, strong "dips" that appear in the diffusive regime.[25] Due to the finite size of the Ag-paint spots, the ballistic regime can be accompanied by fairly low normal-state resistance values, because several parallel microjunctions are actually established between the normal metal and the superconductor, in different points of the apparent contact area. The conductance curves clearly show sharp maxima at energies related to the small gap, Δ_π—even though in the $x=0.2$ case these two peaks are so close that, even at 4.2 K, they cannot be resolved and appear as if they had merged in a single peak at zero bias. Smoother structures related to the large gap, Δ_σ, are also present, such as a shoulder in the first two cases ($x=0$ and $x=0.1$) and a small peak in the third ($x=0.2$). The presence of these structures allows a rough evaluation of Δ_σ, and ensures a greater reliability of the fitting procedure. In the inset of Fig. 6, for example, we report the experimental curve at $x=0.2$, after normalization (i.e., division by the normal-state conductance), together with its fit with the Blonder-Tinkham-Klapwijk (BTK) model generalized to the two-band case[18,26] (solid line), which gives an accurate evaluation of the gap amplitudes. In the main panel of Fig. 6, we plot the so-determined Δ_σ and Δ_π in a selected set of samples ($x=0$, 0.1, and 0.2). Because of the dominant contribution of the π bands to the conductance across the junction even in polycrystalline samples,[27,28] the uncertainty on Δ_σ is generally larger than that on Δ_π, as evidenced by the data summarized in Table II. Note that Δ_σ linearly decreases on increasing Al doping from 7.5 meV at $x=0$ to 3.8 meV at $x=0.2$, which is consistent with the position of the large-gap structures in the conductance curves of Fig. 5. The small gap Δ_π (2.8 meV at $x=0$) shows a decrease in the whole doping range, becoming as small as 1.7 meV at $x=0.2$. In the same figure, we also show the results obtained by specific-heat measurements.[14] The overall agreement between the data as a function of doping is impressive considering the differences inherent to the two experimental techniques (heat capacity measures an average gap throughout the sample, while Andreev reflection probes the gap in a local area close to the surface). Thus PCM in Al-doped samples confirm the previous evidence[14] of the strong decrease of Δ_σ, not accompanied by the predicted[13] rising of Δ_π.

Once the Fermi velocities and the σ-band gap have been estimated as functions of Al doping, it should be possible to scale the experimental critical field curves according to Eq. (2b) (as previously remarked, our experimental values of B_{c2} must be compared with $B_{c2\|ab}$).

In fig. 7, we plot the rescaled critical fields,

$$B_{c2}^{res}(x) = B_{c2}(x)\frac{\Delta_\sigma(0)^2}{\Delta_\sigma(x)^2}\frac{v_{F_{\sigma ab}}(x)}{v_{F_{\sigma ab}}(0)}\frac{v_{F_{\sigma c}}(x)}{v_{F_{\sigma c}}(0)},$$

where $B_{c2}(x)$ is the experimental critical field for each x value and $\Delta_\sigma(x)$ is the linearly interpolated gap. Since B_{c2} is determined by the grains with the lowest doping, Δ_σ was estimated, for each concentration, at the minimum doping in the range $x\pm\Delta x$ of Table I. The values of B_{c2}^{res} have to be compared with the experimental $B_{c2}(0)$ curve (continuous line). The main source of uncertainty on B_{c2}^{res} comes from the

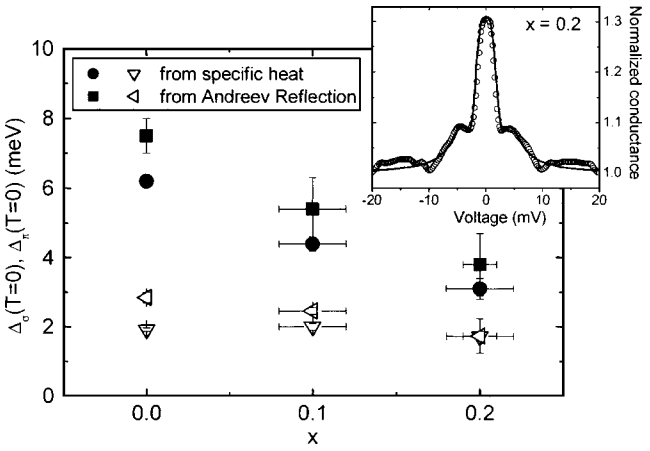

FIG. 6. Main panel: Δ_σ (filled symbols) and Δ_π (open symbols) as a function of x obtained by Andreev reflection and specific-heat data (Ref. 14). Inset: example of a point-contact conductance curve at $T=4.2$ K in the sample with $x=0.2$ (symbols). The line is a two-band BTK fit obtained with the following parameters: $\Delta_\sigma=3.8$ meV and $\Delta_\pi=1.73$ meV, the potential barrier parameters $Z_\sigma=1.55$ and $Z_\pi=0.2$, and the phenomenological broadening parameters $\gamma_\sigma=0.3$ meV and $\gamma_\pi=1.22$ meV. The weight of the π-band conductance was taken equal to 0.75.

ratio between the gaps, which varies by about a factor 2 in the considered range of x. All the curves fall together and overlap with the $B_{c2}(0)$ curve within the experimental uncertainty. Therefore, we can reliably conclude that for $x \leqslant 0.2$, a description within a clean limit model works well.

Further support of our analysis comes from the comparison of the σ-band scattering rates, Γ_σ, with the energy gaps Δ_σ. An estimation of Γ_σ can be made by assuming that the electrical conductivity of Al-doped samples is mainly determined by σ-band carriers. In fact, with the σ orbitals being localized around the B planes, Γ_σ is only slightly affected by substitution in the Mg planes.[4] This hypothesis, although reasonable, provides lower limits for Γ_σ values; however, even if it is relaxed, our conclusions are substantially unchanged. We assume

$$\rho_{0_\sigma} = \Gamma_\sigma/(\varepsilon_0 \omega_{p_\sigma}^2) \approx \rho_0, \tag{3}$$

where ω_{p_σ} is the spatially averaged σ-band plasma frequency and ε_0 is the dielectric constant. The plasma frequencies are given by $\omega_{p_{\sigma i}}^2 = 8\pi(N_\sigma/V_{cell})v_{F_{\sigma i}}^2$ and can be calculated by taking into account the dependence on the Al content of the Fermi velocities, of the density of states N_σ, and of the unit cell volume V_{cell}. The values of $\omega_{p_{\sigma ab}}$, $\omega_{p_{\sigma c}}$, and $\omega_{p_\sigma} = \left(\frac{2}{3}\omega_{p_{\sigma ab}}^2 + \frac{1}{3}\omega_{p_{\sigma c}}^2\right)^{1/2}$ are reported in the lower panel of Fig. 4 as a function of Al doping. As is clearly seen, ω_{p_σ} strongly decreases with the doping due to the filling of the σ bands. An estimation of Γ_σ for the various samples can be obtained from Eq. (3), using the experimental resistivity values and the calculated plasma frequencies. The results are given in Table I. The Γ_σ values weakly increase with Al concentration ranging from 7 to 13 meV. However, the increase of resistivity is mostly accounted for by the decrease of ω_{p_σ}. Finally, in Table I the ratios

$$\frac{\Gamma_\sigma}{\pi\Delta_\sigma} = \frac{\hbar v_{F_\sigma}/\pi\Delta_\sigma}{\hbar v_{F_\sigma}/\Gamma_\sigma} = \frac{\xi_{0_\sigma}}{l_\sigma}$$

are reported. The ratios $\Gamma_\sigma/\pi\Delta_\sigma$ turn out to be lower than 1, confirming that the σ bands in Al-doped samples are in the clean limit for $x \leqslant 0.2$.

TABLE II. Energy gaps and reduced energy gaps of $Al_xMg_{1-x}B_2$ polycrystalline samples.

$x \pm \Delta x$	Δ_σ(meV)	Δ_π(meV)	$2\Delta_\sigma/k_BT_c$	$2\Delta_\pi/k_BT_c$
0	7.5±0.5	2.85±0.01	4.4±0.3	1.70±0.01
0.10±0.02	5.4±0.9	2.5±0.1	3.9±0.8	1.75±0.3
0.20±0.02	3.8±0.9	1.7±0.2	3.0±0.8	1.4±0.5

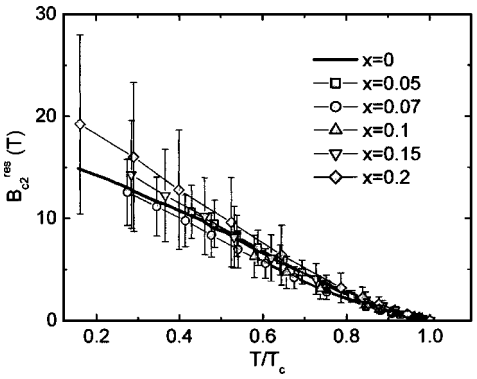

FIG. 7. The rescaled field $B_{c2}^{res}(x)$ as a function of the reduced temperature T/T_c.

In conclusion, in this paper we have discussed the straightforward correlation existing between the critical fields and the σ-band gaps in Al-doped samples. Our main experimental evidence is that B_{c2} monotonically decreases with Al doping while the resistivity increases. On the other hand, we estimated a suppression of Δ_σ with increasing Al doping. This complex phenomenology can be understood by assuming that Al substitution in the Mg sites suppresses the conduction of π bands, but only slightly affects the impurity scattering in σ bands. This makes the clean regime of σ bands particularly robust; in fact, up to $x=0.2$ the upper critical field can be well described within a clean-limit model and its decrease is directly related to the suppression of the superconducting σ gap.

ACKNOWLEDGMENTS

The authors thank S. Massidda, who provided the electronic structure of the Al-doped compound. This work is partially supported by I.N.F.M. through the PRA-UMBRA. V.A.S. acknowledges the support of RFBR (projects No. 04-02-1726 and No. 02-02-17133), Ministry of Science and Technology of Russia (Contract No. 40.012.1.1.1357), and INTAS (project No. 01-0617).

[1] J. Nagamatsu, N. Nakagawa, T. Muranaka, Y. Zenitana, and J. Akimitsu, Nature (London) **410**, 63 (2001).
[2] A. Y. Liu, I. I. Mazin, and J. Kortus, Phys. Rev. Lett. **87**, 087005 (2001).
[3] H. J. Choi, D. Roundy, H. Sun, M. L. Cohen, and S. G. Louie, Phys. Rev. B **66**, 020513(R) (2002).
[4] I. I. Mazin, O. K. Andersen, O. Jepsen, O. V. Dolgov, J. Kortus, A. A. Golubov, A. B. Kuz'menko, and D. van der Marel, Phys. Rev. Lett. **89**, 107002 (2002).
[5] E. Ohmichi, T. Masui, S. Lee, S. Tajima, and T. Osadal, J. Phys. Soc. Jpn. **73**, 2065 (2004).
[6] R. H. T. Wilke, S. L. Bud'ko, P. C. Canfield, D. K. Finnemore, R. J. Suplinskas, and S. T. Hannahs, Phys. Rev. Lett. **92**, 217003 (2004).
[7] V. Braccini, A. Gurevich, J. E. Giencke, M. C. Jewell, C. B. Eom, D. C. Larbalestier, A. Pogrebnyakov, Y. Cui, B. T. Liu, Y. F. Hu, J. M. Redwing, Q. Li, X. X. Xi, R. K. Singh, R. Gandikota, J. Kim, B. Wilkens, N. Newman, J. Rowell, B. Moeckly, V. Ferrando, C. Tarantini, D. Marré, M. Putti, C. Ferdeghini, R. Vaglio, and E. Haanappel, Phys. Rev. B **71**, 012504 (2005).
[8] M. Putti, V. Braccini, C. Ferdeghini, I. Pallecchi, A. S. Siri, F. Gatti, P. Manfrinetti, and A. Palenzona, Phys. Rev. B **70**, 052509 (2004).
[9] O. de la Peña, A. Aguayo, and R. de Coss, Phys. Rev. B **66**, 012511 (2002).
[10] G. Profeta, A. Continenza, and S. Massidda, Phys. Rev. B **68**, 144508 (2003).
[11] P. Postorino, A. Congeduti, P. Dore, A. Nucara, A. Bianconi, D. Di Castro, S. De Negri, and A. Saccone, Phys. Rev. B **65**, 020507(R) (2001).
[12] S. C. Erwin and I. I. Mazin, Phys. Rev. B **68**, 132505 (2003).
[13] A. A. Golubov and I. I. Mazin, Phys. Rev. B **55**, 15 146 (1997).
[14] M. Putti, M. Affronte, P. Manfrinetti, and A. Palenzona, Phys. Rev. B **68**, 094514 (2003)
[15] A. Palenzona, P. Manfrinetti, and V. Braccini, I.N.F.M. patent, No. IT20TO011098 (pending).
[16] B. Birajdar, T. Wenzel, P. Manfrinetti, A. Palenzona, M. Putti, and O. Eibl, Supercond. Sci. Technol. **18**, 572 (2005).
[17] J. S. Slusky, N. Rogado, K. A. Regan, M. A. Hayward, P. Khalifah, T. He, K. Inumaru, S. M. Loureiro, M. K. Haas, H. W. Zandbergen, and R. J. Cava, Nature (London) **410**, 343 (2001).
[18] R. S. Gonnelli, D. Daghero, G. A. Ummarino, V. A. Stepanov, J. Jun, S. M. Kazakov, and J. Karpinski, Phys. Rev. Lett. **89**, 247004 (2002).
[19] I. Pallecchi, V. Braccini, E. Galleani d'Agliano, M. Monni, A. S. Siri, P. Manfrinetti, A. Palenzona, and M. Putti, Phys. Rev. B **71**, 104519 (2005).
[20] B. Kang, H-J Kim, H-S Lee, S-I Lee, and T. Dahm, e-print cond-mat/0403455.
[21] N. R. Werthamer, E. Helfand, and P. C. Hohenberg, Phys. Rev. **147**, 295 (1966).
[22] T. Dahm and N. Schopohl, Phys. Rev. Lett. **91**, 017001 (2003).
[23] P. Miranovic, K. Machida, and V. G. Kogan, J. Phys. Soc. Jpn. **72**, 221 (2003).
[24] D. Di Castro, S. Agrestini, G. Campi, A. Cassetta, M. Colapietro, A. Congeduti, A. Continenza, S. De Negri, M. Giovannini, S. Massidda, M. Nardone, A. Pifferi, P. Postorino, G. Profeta, A. Saccone, N. L. Saini, G. Satta, and A. Bianconi, Europhys. Lett. **58**, 278 (2002).
[25] G. Sheet, S. Mukhopadhyay, and P. Raychaudhuri, Phys. Rev. B **69**, 134507 (2004).
[26] R. S. Gonnelli, D. Daghero, A. Calzolari, G. A. Ummarino, V. Dellarocca, V. A. Stepanov, J. Jun, S. M. Kazakov, and J. Karpinski, Phys. Rev. B **69**, 100504(R) (2004).
[27] A. Brinkman, A. A. Golubov, H. Rogalla, O. V. Dolgov, J. Kortus, Y. Kong, O. Jepsen, and O. K. Andersen, Phys. Rev. B **65**, 180517(R) (2001).
[28] O. V. Dolgov, R. S. Gonnelli, G. A. Ummarino, A. A. Golubov, S. V. Shulga, and J. Kortus, Phys. Rev. B **68**, 132503 (2003).